# CASE STUDY: ANALYSIS OF STIMULATED RESERVOIR VOLUME PROPERTIES THROUGH APPLICATION OF EMBEDDED DISCRETE FRACTURE MODELLING

A Thesis

by

HARI PRASAD ANBALAGAN

Submitted to the Office of Graduate and Professional Studies of
Texas A&M University
in partial fulfillment of the requirements for the degree of

MASTER OF SCIENCE

| | |
|---|---|
| Chair of Committee, | John E. Killough |
| Committee Members, | Eduardo Gildin |
| | Maria Antonieta Barrufet |
| Head of Department, | Jeff Spath |

December 2019

Major Subject: Petroleum Engineering

# ABSTRACT

Hydraulic fracture modelling has always been a challenging task due to the complex network of fractures that have been created in shale and unconventional reservoirs and its associated uncertainty. Primitive modelling of stimulated reservoir volume typically assumes extreme simplifications to hydraulic fractures that do not accurately model the complex dynamic properties of fracture networks. This typically results in large differences in Estimated Ultimate Recovery (EUR) predictions, rendering the history matching workflow less practicable. By applying Embedded Discrete Fracture Modelling (EDFM) in fracture modelling workflow, complex fracture networks can be explicitly modelled without a high computational cost and without the need for any fracture upscaling workflows.

The proposed workflow for given field data exhibits the efficiency of the Embedded Discrete Fracture modelling workflow. The results obtained also showcases the estimated fracture network parameters and its dynamic properties for the field case. The fracture network parameters obtained are also compared against similar cases from literature. The results obtained from EDFM approach is compared against a uniform Stimulated Reservoir Volume (SRV) approach that uses porosity and permeability multipliers and the advantages of EDFM workflow are observed.

DEDICATION

To my parents

ACKNOWLEDGEMENTS

I would like to thank my committee chair, Dr. John Killough, and my committee members, Dr. Eduardo Gildin and Dr. Maria Barrufet, for their guidance and support throughout the course of this research.

Special thanks to Zhi Chai, a former PhD student from Dr. Killough's group, who developed the MATLAB code for Embedded Discrete Fracture Modelling which provided the foundation for this research work.

CONTRIBUTORS AND FUNDING SOURCES

## Contributors

This work was supervised by a thesis committee consisting of Dr. John Killough and Dr. Eduardo Gildin of the Department of Petroleum Engineering and Dr. Maria Barrufet of the Department of Chemical Engineering.

The porosity permeability multiplier model analyzed in Chapter 4 was provided by Dr. John Killough. All other work conducted for the thesis was completed by the student independently.

## Funding Sources

Graduate study was supported by a fellowship from Texas A&M University and Killough Foundation.

# NOMENCLATURE

| | |
|---|---|
| BHP | Bottom Hole Pressure |
| DFM | Discrete Fracture Model |
| EDFM | Embedded Discrete Fracture Modelling |
| NNCs | Non-neighboring connections |
| SRV | Stimulated Reservoir volume |
| TPFA | Two Point Flux Approximation |

TABLE OF CONTENTS

Page

ABSTRACT ..... ii

DEDICATION ..... iii

ACKNOWLEDGEMENTS ..... iv

CONTRIBUTORS AND FUNDING SOURCES ..... v

NOMENCLATURE ..... vi

TABLE OF CONTENTS ..... vii

LIST OF FIGURES ..... ix

LIST OF TABLES ..... xi

1. INTRODUCTION ..... 1

1.1. Conventional Hydraulic Fracture Modelling ..... 1
1.2. Embedded Discrete Fracture Modelling ..... 4
1.3. Research Objective ..... 4

2. OVERVIEW OF EMBEDDED DISCRETE FRACTURE MODELLING ..... 6

2.1. NNC Type I ..... 8
2.2. NNC Type II ..... 8
2.3. NNC Type III ..... 9
2.4. Well and Fracture Intersection ..... 9
2.5. EDFM Preprocessing code ..... 10

3. RESEARCH WORKFLOW ..... 12

3.1. Field Data ..... 12
3.2. Microseismic Data ..... 13
3.3. Diagnostic Fracture Injection Testing ..... 17
3.4. Ensemble generation workflow ..... 17
3.5. History matching ..... 18

4. RESULTS ..... 22

4.1. Initial Ensemble....22
4.2. Ensemble average fracture half-length and heights....23
4.3. Best results....24
4.4. Dynamic SRV analysis....27
4.5. Comparison against a Permeability Porosity multiplier approach....28

5. COMPARING RESULTS WITH LITERATURE....34

5.1. Modeling Interwell Interference Due to Complex Fracture Hits in Eagle Ford Using EDFM (Fiallos, M. X. et al., 2019)....34
5.1.1. Paper Background....34
5.1.2. Similarities between the paper and research work....34
5.1.3. Differences between the paper and research....35
5.1.4. Comparing results....37
5.2. Sampling a Stimulated Rock Volume: An Eagle Ford Example (Raterman, K. T., 2017)....39
5.2.1. Background....39
5.2.2. Some major observations from the paper and comparing the results obtained....39

6. CONCLUSIONS AND DISCUSSIONS....41

REFERENCES....43

LIST OF FIGURES

Page

Figure 1.1: Representation of the heterogeneous porous medium, Warren, J. E., & Root, P. J. (1963) ..... 2

Figure 1.2: Representation of unstructured PEBI grid, Sun, J. et al. (2015) ..... 3

Figure 2.1: Three different types of NNCs Moinfar, A. et al. (2015) ..... 7

Figure 2.2: EDFM pre-processing code workflow, Orta, S.R. (2017) ..... 11

Figure 3.1: Field data well layout ..... 12

Figure 3.2: Illustration of detected microseismicity and the corresponding planar fractures, Shakiba et al. (2015) ..... 13

Figure 3.3: Microseismic cloud of the infill well indicating the primary strike angle ..... 16

Figure 3.4: Microseismic cloud of the infill well indicating the primary dip angle ..... 17

Figure 3.5: Ensemble generation workflow ..... 18

Figure 3.6: Green region shown indicates the microseismic region overlaid on the parent well. The red boxes show the boundary of the fractures for one of the iterations. On the right is the visualization of the EDFM model of the reservoir ..... 19

Figure 4.1: Initial ensemble sample simulation BHP output ..... 22

Figure 4.2: Sample outputs from each ensemble ..... 24

Figure 4.3: Discrete fracture network used for the best history matches ..... 25

Figure 4.4: BHP simulation results for fracture networks modelled using EDFM with fracture heights of 75 ft and 120 ft. ..... 26

Figure 4.5: Fracture conductivity decline curves for case 1 (shorter fracture height) and case 2 (taller fracture height) ..... 27

Figure 4.6: Porosity permeability approach multiplier applied to estimated SRV ..... 28

Figure 4.7: Simulation Result of permeability porosity multiplier approach ..... 29

Figure 4.8: Oil production rates for 5 year simulation run for multiplier approach and EDFM cases ..... 30

Figure 4.9: Cumulative Oil Production for 5 year simulation runs ..... 31

Figure 4.10: Cumulative Gas Production for 5-year simulation runs ..... 32

Figure 4.11: Average pore pressure vs production period for multiplier approach and EDFM approach ..... 33

Figure 5.1:Permeability and porosity values for the field case used in the paper (Fiallos, M. X. et al., 2019) ..... 35

Figure 5.2: Parent and child well layout of Eagle Ford case. Fracture planes are modelled as planes (Fiallos, M. X. et al., 2019) ..... 36

Figure 5.3: BHP production history and EDFM simulation of Eagle Ford case (Fiallos, M. X. et al., 2019) ..... 37

Figure 5.4: EDFM model parameters after successful history match for Eagle Ford case (Fiallos, M. X. et al., 2019) ..... 38

LIST OF TABLES

Page

Table 2.1 NNC Formulations ..... 7

Table 3.1: Reservoir grid parameters ..... 21

Table 3.2: Fracture network parameters ..... 21

Table 4.1: Reservoir gridblock Parameters ..... 23

Table 4.2: Fracture Parameters ..... 25

# 1. INTRODUCTION

## 1.1. Conventional Hydraulic Fracture Modelling

Hydraulic fracturing of ultra-low permeability formations has been the vehicle that has led to the US shale revolution. Hydraulic fracturing creates highly conducive flow pathways and increase the effective reservoir volume that is in contact with the reservoir. In cases of multi-phase flow, fractures may create highly conductive flow corridors which may lead to unexpected high water cut and high GOR. Hence, for efficient extraction of oil and gas reserves in unconventional reservoirs, accurate fracture modelling becomes critical. Conventional methods that have been proposed to study flow in fractured reservoirs include dual continuum models and discrete fracture modelling.

The dual continuum method involves orthogonal structured gridding of both matrix and the up-scaled fracture systems, as shown in Fig 1.1, in which cubical cells are often used to represent the fractures. Owing to their simplistic representation, they fail to accurately model problems with multi-scale, slanted, irregularly spaced, non-uniform fractures. This approach treats fractures as a continuous porosity type where fracture properties are upscaled to a coarser grid of scale similar to the matrix. This approach is suitable for a small set of cases with small scale fractures that are well connected. However, large error could be observed for cases with large fractures dominating the flow and is hence not a practicable approach in most cases based on studies such as Gillespie,

P. A. et al. (1993), Ouillon, G. et al. (1996), Aarseth, E. S. et al. (1997), Odling, N. E. et al (1999), Gale, J. F. et al. (2014).

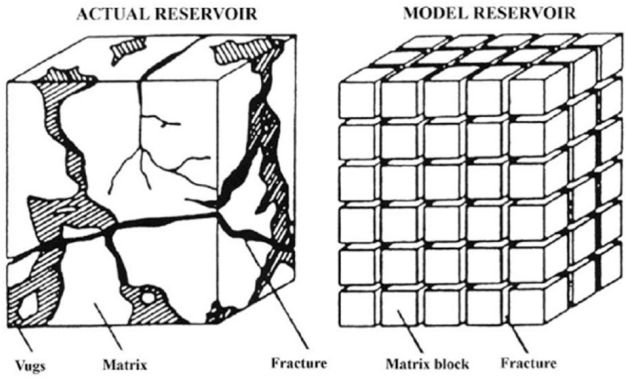


**Figure 1.1: Representation of the heterogeneous porous medium, Warren, J. E., & Root, P. J. (1963)**

Discrete fracture models (DFMs), on the other hand, capture more complex configurations associated with natural and hydraulic fractures by using unstructured elements, such as polygons and polyhedron cells. To conform to the geometry of fractures, the gridding algorithms refine the grid cells as it gets closer to the fracture planes. The advantage for DFMs as compared to dual porosity models is that the influence of fractures can be directly incorporated in the model, without the need to assume any abstract property of the fracture network.

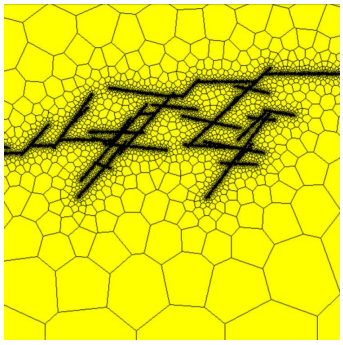

**Figure 1.2: Representation of unstructured PEBI grid, Sun, J. et al. (2015)**

The perpendicular bisector grid (PEBI) model is one common type of DFM and a representation is shown in Fig 1.2. It was introduced to reservoir simulation by Heinemann, Z. E. et al. (1989) and has been a popular approach for fractured reservoir simulation. The flux direction is perpendicular to the grid boundary, thus ensuring accuracy when applying two-point flux approximation (TPFA). Karimi-Fard, M. et al. (2004) proposed a discrete fracture model with unstructured gridding to explicitly represent the fractures and to account for the mass transfer between grid blocks used two-point flux approximation method. Sandve, T. H. et al. (2012) extended the method from two-point flux approximation to multiple point approximation and obtained improved accuracy. However, it can be computationally challenging to generate the unstructured grid that conforms to the fracture geometry. Mustapha, H. (2014) showed that mesh quality often degrades with large number of tiny grid blocks, which is often the case for a complex fracture configuration. There is an unintended consequence of high computational cost due to larger amount of computational grid blocks associated with DFMs as well. This disadvantage posed by DFMs make it practically unfeasible to run large number of simulations, especially during history matching for field cases.

## 1.2. Embedded Discrete Fracture Modelling

The Embedded Discrete Fracture Model (EDFM) was originally proposed by Lee, S. H. et al. (2000) and Li, L., & Lee, S. H. (2008) to solve the limitations associated with dual continuum and discrete fracture models and to take advantage of the synergy between the two methods. In EDFM, fracture planes are inserted explicitly in the matrix grid and are discretized by the cell boundaries. The matrix and intersecting fractures are then connected by non-neighboring connections (NNCs), which provides for fluid flow between the fractures and the grid blocks. The advantages of EDFM over traditional modelling methods are that it is computationally inexpensive and can accommodate a discrete fracture network model.

## 1.3. Research Objective

The objective of this thesis is to analyze the dynamic properties of the SRV for the field case provided. History matching of Bottom Hole Pressure (BHP) for the parent well up to 479 days will be performed which will in turn help to estimate the following:

1. Complex fracture network properties such as half-length, fracture width, fracture spacing, dip and strike angles and the stimulated reservoir volume observed for the parent well
2. Fracture conductivity and its dynamic behavior over depletion time
3. Computational efficiency of EDFM for fracture modelling and history matching

Additionally, the results obtained through EDFM workflow are compared against results in existing literature. Results obtained are also compared against a simplistic workflow that involves modifying SRV parameters such as porosity and permeability. The thesis seeks to provide a platform for future studies on history matching for the infill wells in the same field which in turn can help to understand fracture hits and well interference in unconventional wells.

# 2. OVERVIEW OF EMBEDDED DISCRETE FRACTURE MODELLING

The concept of EDFM, first proposed by Lee, S. H. et al. (2000) and Li, L. et al. (2008) discretizes the matrix without the need to consider the fractures. Fractures are discretized by the boundary of the matrix grid blocks. The transmissibility between fracture and the matrix similar to the calculation of well index. In the calculation of well index, the relationship between well cell pressure and bottom-hole pressure is derived based on radial flow assumption. Likewise, by assuming a linearly distributed pressure in the vicinity of fractures, an analytical expression of the transmissibility can be obtained between the fracture cell and the matrix cell.

As fracture geometry has no impact on the matrix grid, this method allows for complex fracture network to be incorporated in any matrix grids. Compared to PEBI model, computationally expensive procedures such as the Delaunay triangulation which are required to generate the unstructured grids surrounding the fracture can be avoided resulting in a much smaller computational problem to solve. Compared to dual-continuum models, EDFM has significantly improved accuracy due to fractures being explicitly defined devoid of any fracture upscaling procedures.

In EDFM implementation, three types of non-neighbor connections (NNCs) are considered to connect the fracture grids with the rest of the reservoir defined as below

1. Between fracture and the matrix grid, inside which the fracture is located
2. Between two intersecting fracture grids
3. Between two neighbor fracture grids arising from the same fracture.

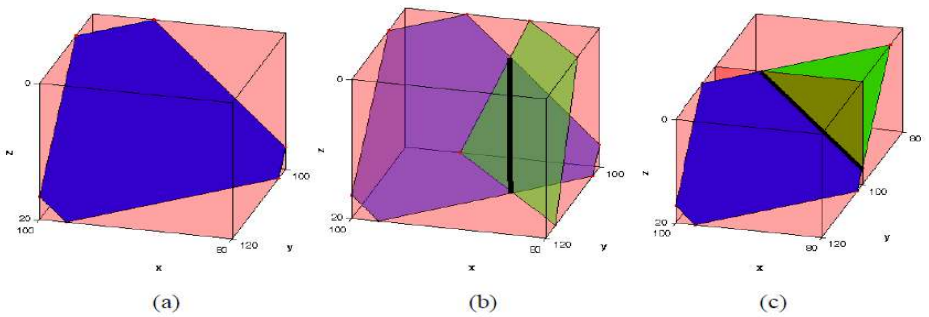


**Figure 2.1: Three different types of NNCs Moinfar, A. et al. (2015)**

Fig 2.1 shows the representation of the different types of NNCs. The formulations to calculate the transmissibility for each type of non-neighbouring connections are summarized in Table 2.1. The details of the calculation are shown in subsequent sections.

**Table 2.1 NNC Formulations**

| NNC Type | $T_{NNC}$ | $k_{NNC}$ | $A_{NNC}$ | $d_{NNC}$ | $T_i$ |
|---|---|---|---|---|---|
| I | $\frac{A_{NNC}k_{NNC}}{d_{NNC}}$ | $\frac{2}{{k_f}^{-1} + {k_m}^{-1}}$ | $A_{frac}$ | $d_{norm\,avg} = \frac{\int_V x_n\, dv}{V}$ | --- |
| II | $\frac{1}{{T_1}^{-1} + {T_2}^{-1}}$ | --- | --- | --- | $\frac{k_{f_i}w_{f_i}L_{int}}{d_{f_i}}$ |
| III | $\frac{1}{{T_1}^{-1} + {T_2}^{-1}}$ | --- | --- | --- | $\frac{k_{f_i}w_{f_i}L_{int}}{d_{f_i}}$ |

## 2.1. NNC Type I

For a NNC between matrix and fracture cells (Figure 2.1a), $A_{NNC}$ is the surface area of the fracture inside the gridblock. Fluid transfer between the fracture and matrix takes place through this surface. $k_{NNC}$ (NNC permeability) is taken as the harmonic average of the matrix and fracture permeabilities. Typically, $k_{NNC}$ is close to the matrix permeability as in most cases fracture permeability is significantly larger than matrix permeability.

To calculate $d_{NNC}$, Li, L., & Lee, S. H. (2008) and Hajibeygi, H. et al. (2011) assumed that the pressure varies linearly in the normal direction to each fracture in a gridblock and proposed the following equation for computing the average normal distance (<d>):

$$< d_n > = \frac{\int_V x_n dv}{V}$$

where $\int_V$ , $x_n$, and $dv$ are the volume element, the normal distance of the element from the fracture, and volume of a gridblock, respectively. This is calculated in the pre-processing code.

## 2.2. NNC Type II

For a NNC between two intersecting fracture segments Karimi-Fard, M. et al. (2004) calculated the transmissibility as

$$\frac{A_{NNC} k_{NNC}}{d_{NNC}} = \frac{1}{{T_1}^{-1} + {T_2}^{-1}}$$

$$T_1 = \frac{k_{f_1} w_{f_1} L_{int}}{d_{f_1}},$$

$$T_2 = \frac{k_{f_2} w_{f_2} L_{int}}{d_{f_2}}$$

where $L_{int}$ is the length of the intersection line bounded in a gridblock (black solid line in Figure 2.1b). $d_f$ is the average of normal distances from the center of the fracture subsegments to the intersection line.

### 2.3. NNC Type III

For NNC between two cells of an individual fracture, $k_{NNC}$ is the fracture permeability and $d_{NNC}$ is the distance between the centers of two fracture segments. The black solid line in Figure 2.1c represents the intersection line of the fracture plane and the common face of two neighboring grid blocks. Parameter $A_{NNC}$ is the fracture aperture times the length of the intersection line.

### 2.4. Well and Fracture Intersection

An accurate well model is required to relate the well rate to the well pressure and the pressure of fracture intersecting the well as it has the highest influence on well productivity. Peaceman, D.W. (1983) established a mathematical model between the well block pressure and the wellbore pressure for a vertical well. The Peaceman's well index (WI) for a vertical well, which is used in most reservoir simulators, is given by

$$WI = \frac{kh}{ln(\frac{r_o}{r_w})}$$

$$where\ r_o = \frac{0.28\sqrt{\left(\frac{k_y}{k_x}\right)^{0.5}\Delta x^2 + \left(\frac{k_x}{k_y}\right)^{0.5}\Delta y^2}}{\left(\frac{k_y}{k_x}\right)^{0.25} + \left(\frac{k_x}{k_y}\right)^{0.25}}$$

where $k_x$ and $k_y$ are the permeability in the x and y directions, respectively, and Δx and Δy are the horizontal dimensions of the well block. k, h, and $r_w$ are the well block permeability, the well block height (identical to the length of well in the gridblock), and the wellbore radius, respectively. In EDFM, depending on well-fracture geometric configuration, the Peaceman's well model is modified by Moinfar, A. et al. (2014) to derive a relationship for the well-fracture intersection as below

$$WI_f = \frac{k_f w_f}{ln(\frac{r_o}{r_w})}$$

$$r_o = 0.14\sqrt{{L_f}^2 + {h_f}^2}$$

where $k_f$ is the fracture permeability, $w_f$ is the fracture aperture, $L_f$ is the fracture length bounded in the gridblock and $h_f$ is the fracture height in the same gridblock.

### 2.5. EDFM Preprocessing code

The MATLAB preprocessor code was developed by Zhi Chai as part of Dr. Killough's research group. A simplistic workflow of the preprocessor code is shown in Fig 2.2.

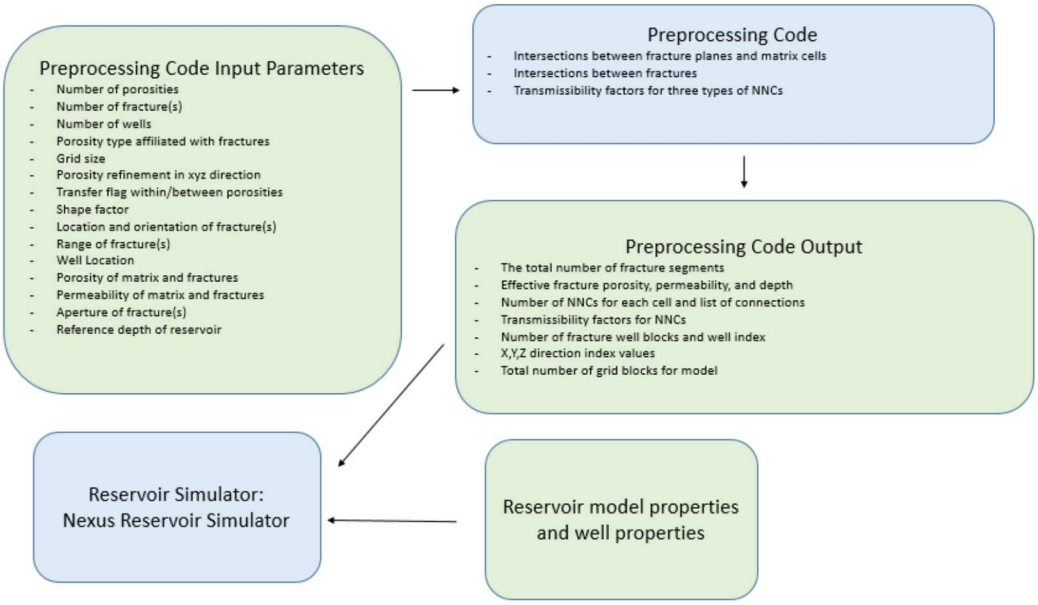


**Figure 2.2: EDFM pre-processing code workflow, Orta, S.R. (2017)**

The preprocessor was modified to take information from the upscaled grid (for the given field data) including permeabilities ($k_x, k_y, k_z$), porosities, initial saturation and pressure maps from Landmark Nexus. The fracture code was modified to write additional output files that have pressure and saturation initializations for the fractures and the rest of the matrix grid. Additionally, the preprocessor is modified to differentiate fracture elements that intersect with the well.

# 3. RESEARCH WORKFLOW

## 3.1. Field Data

Field data is available for an ultralow permeability primarily black oil field. The field consists of parent horizontal well (labelled W1 in Fig 3.1) and multiple infill horizontal well (labelled W2-W7 in Fig 3.1). The parent well was in production for 479 days after which the infill wells were drilled. The history matching workflow is performed for the parent well, during which it is the only well in operation in the field. This reduces the problem complexity, as infill well depletion and fracture hits are not factored into this problem. As the parent well does not have a BHP gauge, the BHP is calculated based on the wellhead pressure, gas and oil flow rates at the surface. The history match is performed by varying the fracture network parameters with the objective to match the observed calculated BHP by constraining the simulation models to the observed oil production rates.

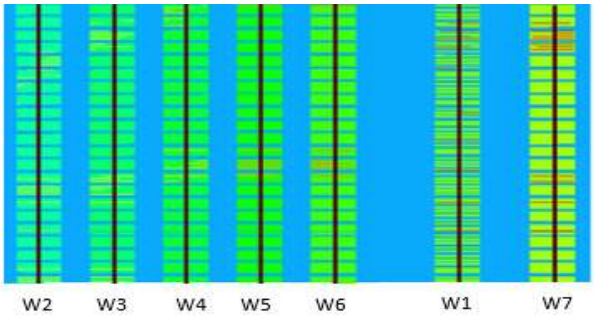


**Figure 3.1: Field data well layout**

### 3.2. Microseismic Data

Microseismic monitoring during hydraulic fracturing of unconventional wells aids to translate the received seismic information into a fracture network model for further simulation of production and reservoir depletion. The distribution of microseismic events helps to evaluate the size and complexity of the fracture system. If the aspect ratio of width to length of microseismic events, called microseismic cloud aspect ratio, is low, then this configuration can be categorized by simple planar fractures. In this situation, the distribution of microseismic events assists in quantifying the dimensions of planar hydraulic fractures (half-length and height). Fig. 3.2 represents a synthetic illustration of the detected microseismicity and the corresponding planar fractures.

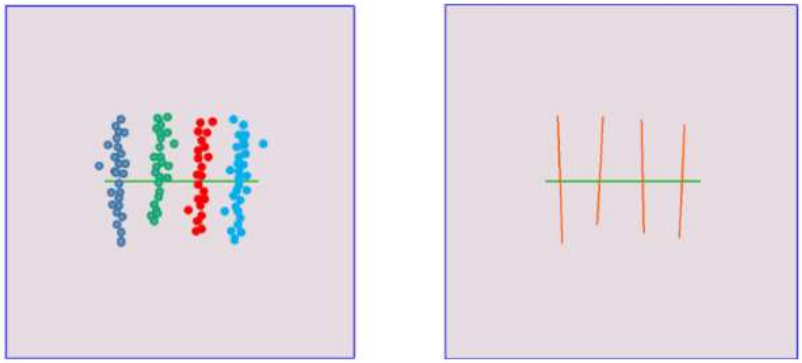

**Figure 3.2: Illustration of detected microseismicity and the corresponding planar fractures, Shakiba et al. (2015)**

On the other hand, if the microseismic cloud aspect ratio is high indicating a highly diffused pattern then the treatment is described as a complex fracture network (Cipolla, C.L. et al. 2008). Fitting a planar fracture to such a trend may result in misleading

interpretations. Although the overall volume of the recorded events provides an initial estimate of the spatial extent of the stimulated zone, it has little information about the efficiency of the fracture network and fluid placement. Indeed, a stimulation job with a large microseismic cloud would not increase the productivity of the well, if the hydraulic connectivity and the distribution of conductivity are poor inside the network. To distinguish between the total microseismic volume and the productive subset of the fracture network, the term effective stimulated reservoir volume (SRV) is often applied. In such situation, it is very crucial to have an idea of the complexity and geometry of the fracture system to ensure a reliable production forecast.

With recent advancements in fracture diagnostic techniques, it has been established that a complex fracture geometry often occurs in shale reservoirs. (Wu, K. and Olson, J. E., 2016). The complex fracture geometry results in non-uniform spatial drainage volume along the wellbore, which significantly affects fracture design and well spacing optimization (Yu, W. et al., 2017). Hence, simple fracture geometries such as bi-wing planar fractures and orthogonal fracture networks, which are used in the reservoir simulation, are inadequate to capture the complex nature of fracture geometry.

Microseismic recordings were initially assumed to be based on shear waves. However, some recent studies report variable microseismic source mechanisms during hydraulic fracturing ranging from shear to tensile failures and including components in between (Seibel, M. et al., 2010). Hence understanding the source mechanism during hydraulic fracturing becomes critical to image the fracture network accurately.

In a typical workflow, a subset of high-quality recorded microseismic data (with high signal-to-noise ratio and amplitude) are used to build a complex fracture network. The source mechanics of rock failure are measured for every microseismic event by various designs of surface-monitoring arrays. During construction of the fracture network in simulation, fracture planes are placed at the location of high quality microseismic events, while the area and aperture of the fractures are estimated based on event magnitude (Kanamori, H., 1977). Fracture orientation is typically determined from source-attributes characterization (Williams-Stroud, S.C., 2008). This workflow is feasible only if large amount of high-quality data is available. This is typically possible only when a multi-well array system is used as a single observation well has shortcomings with respect to determination of accurate fracture geometries and location. (Seibel, M. et.al, 2010).

For the dataset used in this research, single well array microseismic is available for one of the infill wells (W6). As the microseismic data is not derived from a multi well array and the data does not belong to the parent well, there is limited information about the possible fracture network of W1 that can be garnered by studying the microseismic cloud of W6. Those include the following:

1. As the completion zone is the same for both the wells, information such as primary fracture strike and dip angles can be extracted from the microseismic data of W6
2. The microseismic cloud shows the fracture density variation along the length of the well. Regions of extremely large half lengths are ignored as they could be attributed to fracture hits as the microseismic data belongs to an infill well. This

information broadly serves the starting point of the half lengths of fracture planes for initial ensembles

3. The cloud aspect ratio is used to deduce the complexity of the fracture network

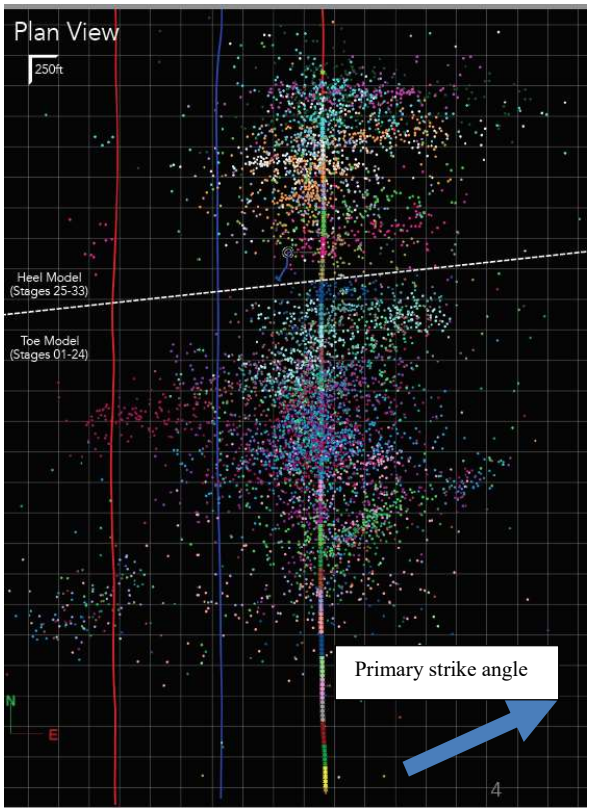


**Figure 3.3: Microseismic cloud of the infill well indicating the primary strike angle**

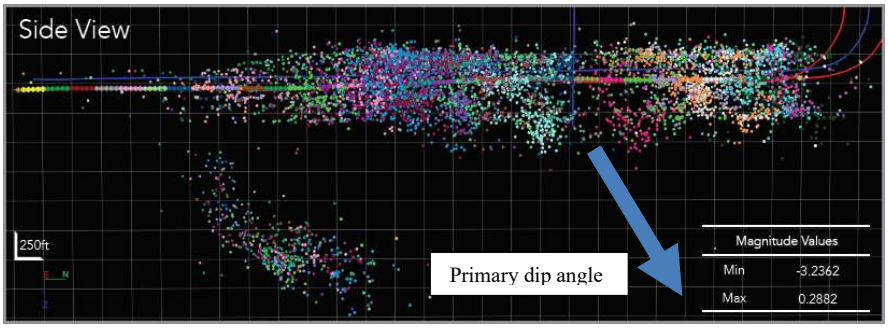


**Figure 3.4: Microseismic cloud of the infill well indicating the primary dip angle**

### 3.3. Diagnostic Fracture Injection Testing

Diagnostic Fracture Injection Testing is a short duration, small volume fracturing operation where a small amount (typically less than hundred barrels) of water is pumped until fracture initiation. At this point, the valve is closed allowing the well's pressure to fall-off naturally over the course of 24 to 48 hrs. This test provides an estimate of the fluid leak-off coefficient as well as fracture initiation and fracture closure pressures.

### 3.4. Ensemble generation workflow

By using fluid leak-off coefficient estimated, and with information pertaining pad and proppant injection time, injection volume, and approximations made with regards to porosity of fracture network, the fracture width of a fracture network configuration for a particular ensemble is calculated.

Typical average fracture widths in shale formations range between 0.1 – 0.5 inches (Siriwardane, H. et al., 2016). Fracture networks that generate fracture width larger than 0.5 inches are ignored and not considered as part of the ensembles. Different sets of

fracture networks are created based on all the above information. A simple workflow chart is shown in Fig 3.5.

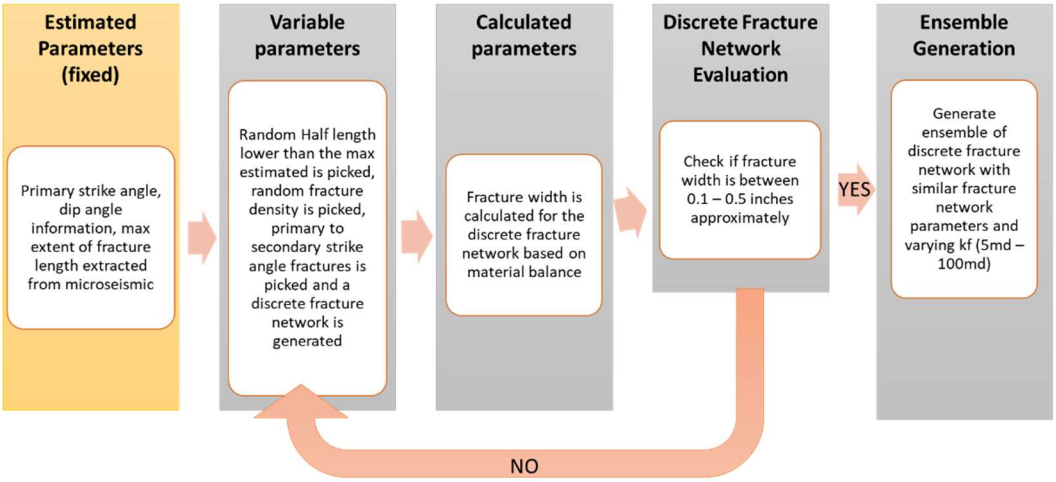


**Figure 3.5: Ensemble generation workflow**

Based on the workflow, a pictorial representation of one of the outputs from one of the ensembles is shown in Fig 3.6

### 3.5. History matching

History matching is broadly defined as the process of building a set of numerical simulation models (representing a reservoir) which reasonably account for observed and measured data. For a given ensemble of fracture network models, the EDFM preprocessor developed by Dr. Killough's group is used to generate the simulation data files in MATLAB. The simulation is executed in Landmark Nexus. After studying the results and the global error percentage average for every model of every ensemble, the fracture

network properties are varied for the next ensemble. This process is continued until a good match is obtained (approx. 30% or lower global error percentage.)

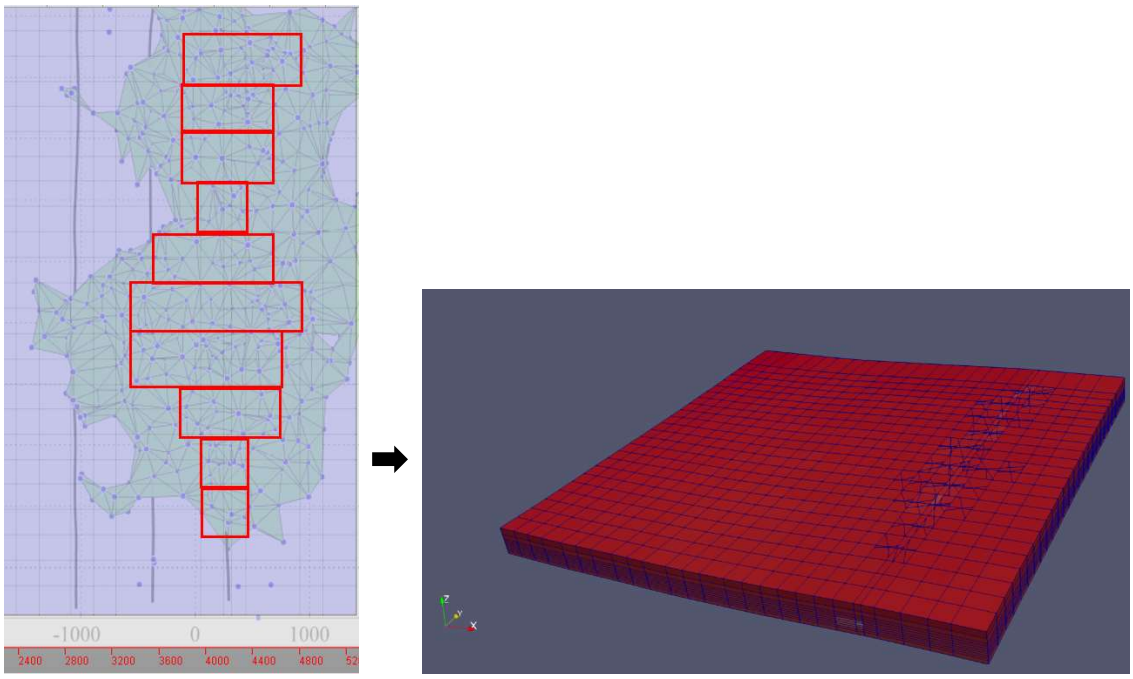


**Figure 3.6: Green region shown indicates the microseismic region overlaid on the parent well. The red boxes show the boundary of the fractures for one of the iterations. On the right is the visualization of the EDFM model of the reservoir**

As the workflow involves manual input control (for the purposes of discrete fracture network) in MATLAB and the generated files are manually input into Nexus Simulation projects, the workflow is cumbersome to be automated and hence a manual history matching method is employed with the sole objective of the history match process to reduce global error percentages by varying fracture network properties for a given upscaled reservoir grid.

Certain assumptions are made to simplify the manual history matching process without adversely impacting the results.

1. All fractures are assumed to have the same properties – fracture conductivity, fracture conductivity variation with pressure and transmissibility variation with pressure.
2. The fracture network is used to model only fractures that are propped. As unpropped fractures are typically large in unconventional wells in shale formations and do not contribute significantly to well productivity (Zheng, S. et al., 2019)
3. Unpropped fractures are not modelled as part of the discrete fracture network. This is attributed to the early fracture closure of the unpropped fractures and fracture conductivity that is 3-4 times lower in magnitude as compared to propped fractures. (Wu, W. et al., 2017)

The reservoir simulation grid parameters are summarized in Table 3.1 and fracture network parameters are summarized in Table 3.2.

**Table 3.1: Reservoir grid parameters**

| Parameter | Range/ Value | Type |
|---|---|---|
| Grid Size | 26 x 24 x 11 | Fixed |
| Field Dimensions | 5200 ft x 4500 ft | Fixed |
| Initial gridblock pressures | 3161 – 3265 psia | Fixed |
| Initial water saturation | 0.442-0.52 | Fixed |
| Initial Gas Saturation | 0 | Fixed |
| **Parameter** | **Range/ Value** | **Type** |
| Porosity | 2.7-7% | Fixed |
| Permeability | 0.3-0.9 μd | Fixed |

**Table 3.2: Fracture network parameters**

| Parameter | Range/ Value | Type |
|---|---|---|
| Fracture Permeability | 5md – 100 md | *Simulation Variable* |
| Fracture Half Lengths | 1500ft – 50ft | *Simulation Variable* |
| Fracture Heights | 300ft – 50ft | *Simulation Variable* |
| Conductivity vs pressure | NA | *Simulation Variable* |
| Fracture Width | Calculated for every simulation run, constrained between 0.1-0.5 inches | Fixed for every configuration, based on mass balance of fluid pumped |

# 4. RESULTS

## 4.1. Initial Ensemble

The initial ensemble consists of large fracture network characterized by fracture half lengths ranging between 500 – 1500 feet and fracture heights between 250-300 feet. The initial ensemble has a fracture network that is bound between the red boxes shown in Fig 3.6. The results of the same output are shown in Fig 4.1.

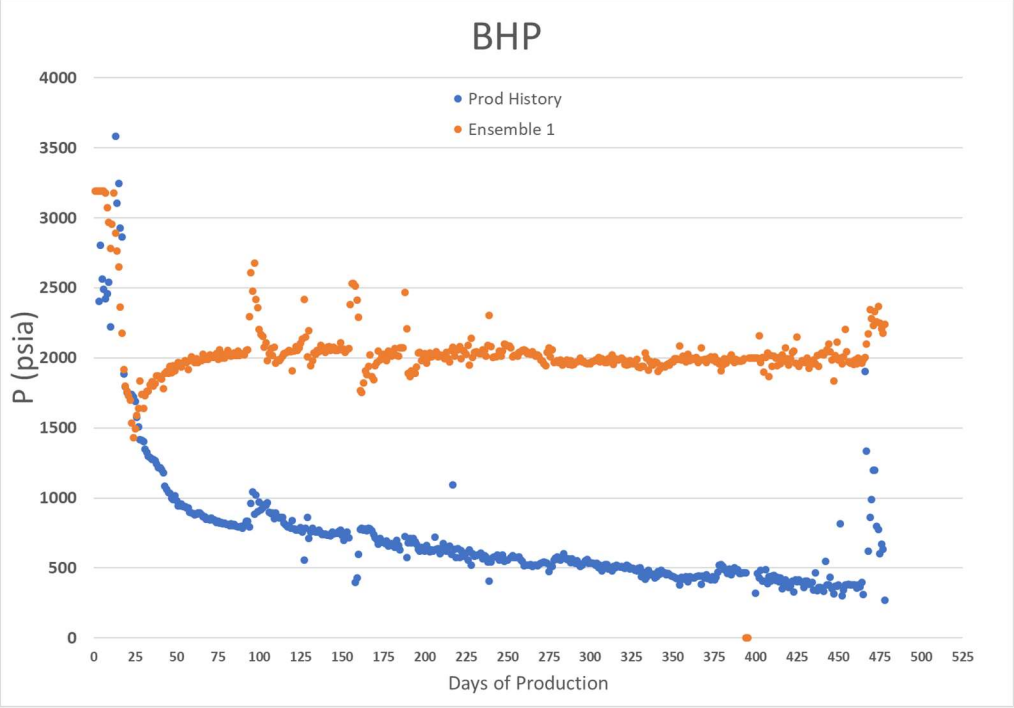


**Figure 4.1: Initial ensemble sample simulation BHP output**

A study of the simulated BHP curve yields understanding of the parameters to vary. After the initial rapid decline up to 25 days, the BHP starts to increase again indicating the reservoir simulation model is showcasing a rapid buildup of oil at bottom

hole conditions, higher than the oil being produced at well head conditions. This means that the stimulated reservoir volume indicated by the simulation model is much larger than actual. This leads to reducing the fracture half lengths and fracture heights in subsequent ensembles. However, when the fracture half lengths and heights are reduced, the number and density of fractures is increased to maintain similar total fracture network area such that the calculated fracture width is still within the range of 0.1- 0.5 inches.

### 4.2. Ensemble average fracture half-length and heights

Based on the above, four ensembles are generated. Each ensemble typically has a set of similar fracture networks with varying fracture permeabilities. Fig 4.2 shows a single BHP output from one of the configurations from each of the ensembles.

**Table 4.1: Reservoir gridblock Parameters**

| Ensemble # | Half Length Range (ft) | Fracture Height Range (ft) | Global error average % Range |
|---|---|---|---|
| 1 | 500-1500 | 250-300 | 350-400 |
| 2 | 250-750 | 200-250 | 180-300 |
| 3 | 100-400 | 100-150 | 50-150 |
| 4 | 50-100 | 75-100 | 70-90 |

We can notice in Fig 4.2 that the samples from ensembles 3 and 4 are the closest match to the BHP match. The parameters varied did not include variation of the conductivity decline with pressure, with a linear decline assumed for all simulation runs for all cases.

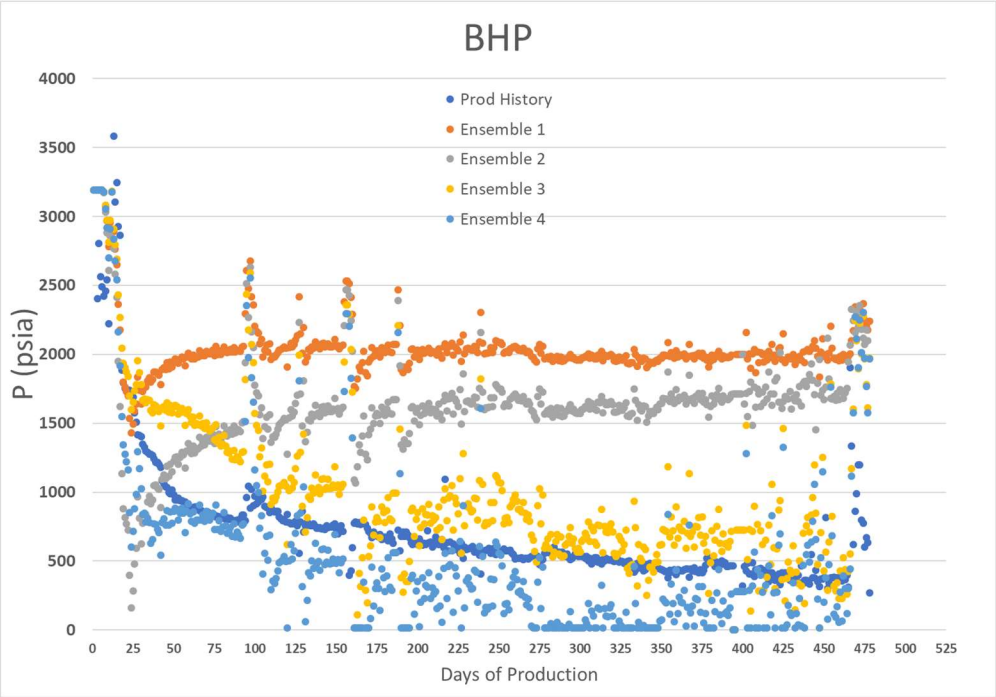


**Figure 4.2: Sample outputs from each ensemble**

With the results obtained from linear conductivity decline, different models from ensembles 3 and 4 are picked and an exponential conductivity decline is tested. With improved results obtained, the exponential conductivity decline parameters are varied until the best match is obtained. The best conductivity decline is then applied to different models in ensemble 3 and 4 to check for improved results.

### 4.3. Best results

Two good results are obtained with the parameters and error percentages shown in table 4.2. A pictorial representation of the fracture network is shown in Fig 4.3. The BHP

results are shown in Fig 4.4 and the fracture conductivity decline is shown in Fig 4.5. Simulation BHP responses are typically higher than the production history observed, when the well is shut in for short periods of time.

**Table 4.2: Fracture Parameters**

| Parameter | Range/ Value |
|---|---|
| Initial Fracture Conductivity | 8 – 13 md.ft |
| Fracture Half Lengths | 100- 125 ft |
| Fracture Heights | 75ft -120 ft |
| Fracture conductivity vs pressure | Shown in Fig |
| Global average error percentage | 24% - 29% |

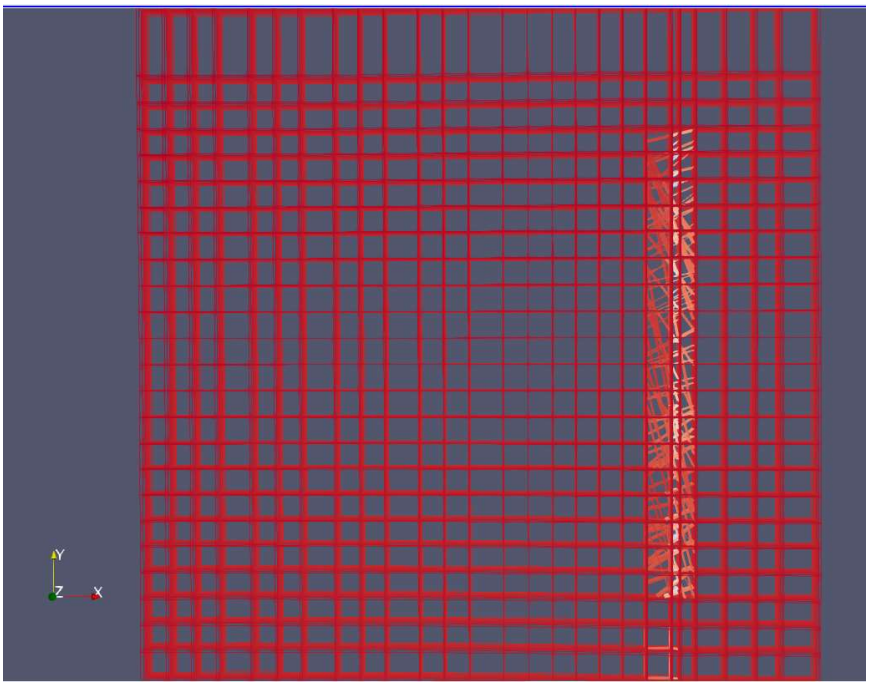


**Figure 4.3: Discrete fracture network used for the best history matches**

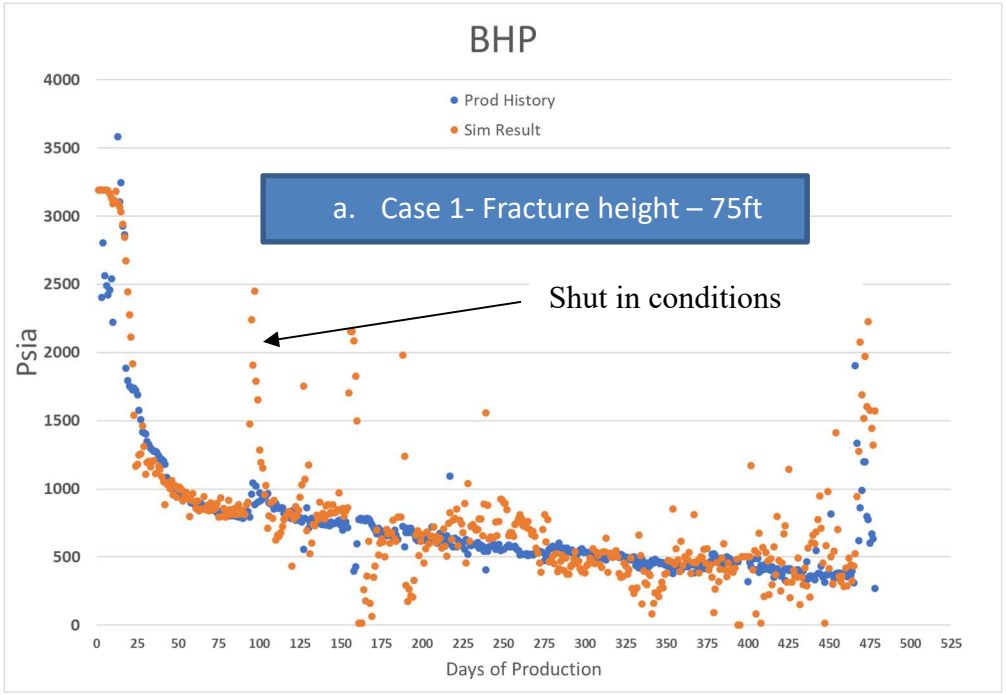


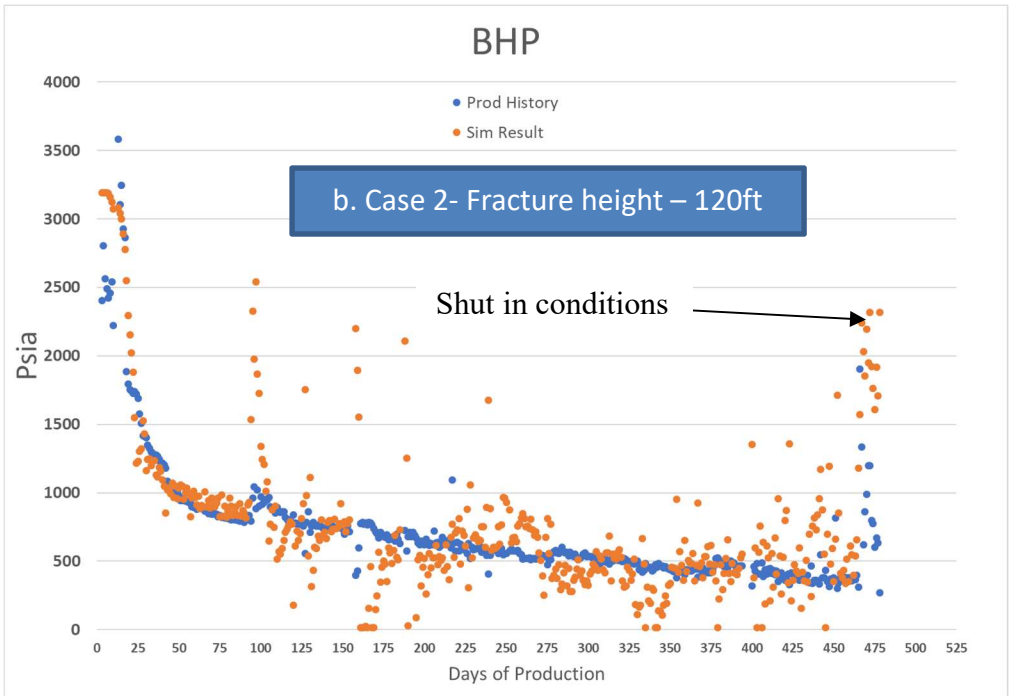


**Figure 4.4: BHP simulation results for fracture networks modelled using EDFM with fracture heights of 75 ft and 120 ft.**

### 4.4. Dynamic SRV analysis

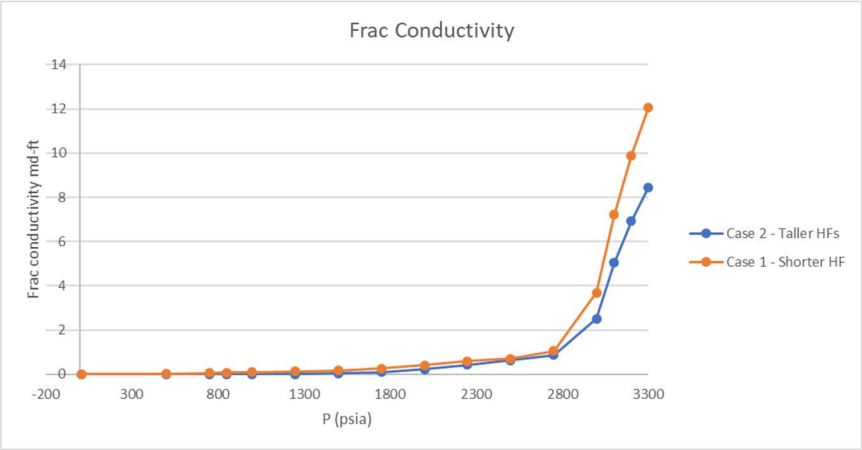


**Figure 4.5: Fracture conductivity decline curves for case 1 (shorter fracture height) and case 2 (taller fracture height)**

The fracture conductivity decline curve shows that the initial fracture conductivity decline is sharp, indicating that production rates also drop significantly with fracture pressure decline. The conductivity decline curve also explains the more gradual BHP decline after 50 days of production. For example, at 50 days, the average pressure of fracture elements is around 2800 psia. With initial fracture pressures around 3250 psia, the rapid decline of fracture conductivity by a factor of 8-10 indicate that fractures no longer provide good conduits for oil flow after 50 days. This is also evidenced by oil production rates dropping to an average of 300 STB/day after 50 days of production from 1000 STB/day immediately after production started. Physically, this conductivity decline could be attributed to closure of fracture width and decreasing effective fracture permeability.

### 4.5. Comparison against a Permeability Porosity multiplier approach

A simplified history matching approach for unconventionals is to model parallel fracture planes spaced along the horizontal well. The fracture planes re modelled to have a significant higher permeability than the grid blocks. Additionally, the estimated SRV region grids have a modified porosity and permeability to model the BHP response observed. This gives a good indication of the SRV volume and its depletion until the production history. This approach was performed within the research group and is not a part of this workflow. However, the results are compared against EDFM results obtained. Fig 4.6 shows the bounding box within which the multipliers were applied, and Fig 4.7 shows the BHP response of the simulation.

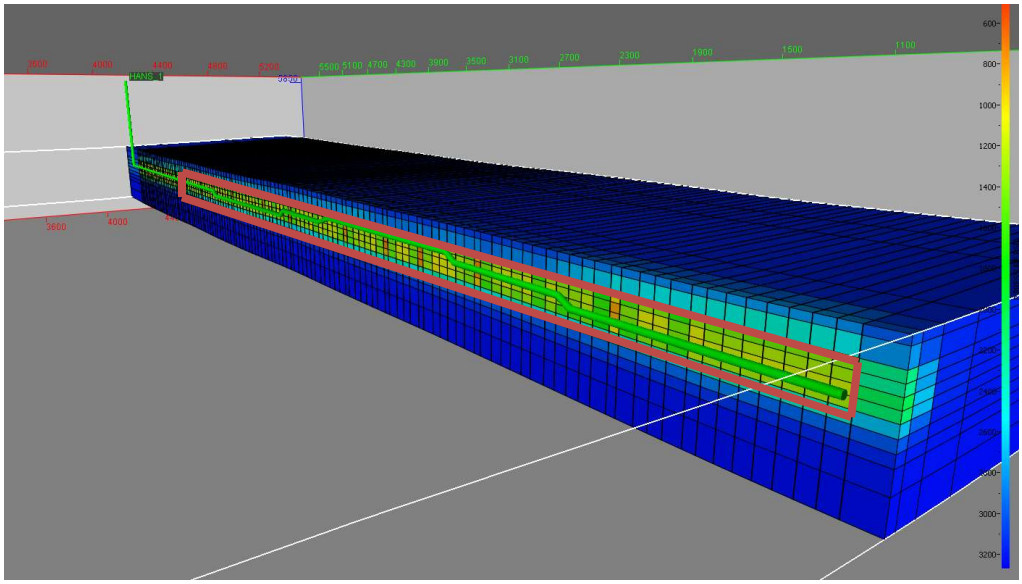

**Figure 4.6: Porosity permeability approach multiplier applied to estimated SRV grid blocks**

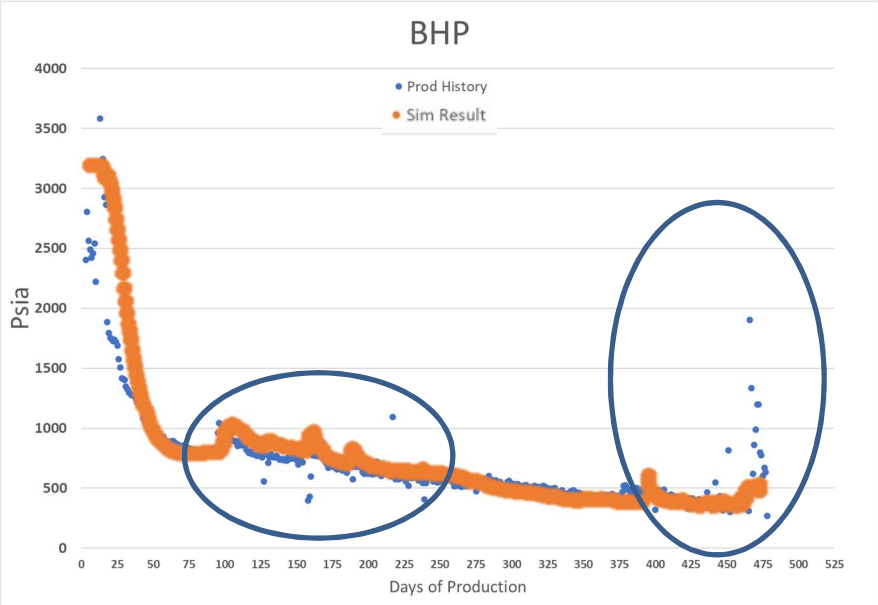


**Figure 4.7: Simulation Result of permeability porosity multiplier approach**

With a significantly better match (global average error percentage around 5%) than the EDFM approach, it may be tempting to assume that the multiplier approach provides a better framework to study the depletion. It is seen that the pressure response observed is smoothed out and does not reproduce accurately pressure responses during shut in periods when the BHP rapidly increases (shown in circles in Fig 4.7), which indicates that the fracture network is not accurately modelled in the event of multiplier approach. This is because of the uniform multipliers that are applied throughout the SRV which is physically not possible to achieve, as a fracture network that exists over a range of 5000 feet is bound to have regions of high and low depletion. This drawback of the uniform multiplier approach in modelling multi-well cases, where the one of the primary reasons to perform history matching is to study fracture hits and well interference.

For purposes of comparison of forecasting accuracy of the multiplier approach with the EDFM cases, the simulation is run with BHP fixed at 450 psia for a period of up to 5 years after 479 days of production. Fig 4.8 shows the oil production rates observed. Oil production rate being an input data for the simulations, the rates match perfectly for all three cases up to 479 days. After that, the cases are switched to constant BHP. EDFM history match cases, case 1 (fracture height of 75 feet) and case 2 (fracture height of 120 feet), have higher oil production rates for most part of the 5 year period.

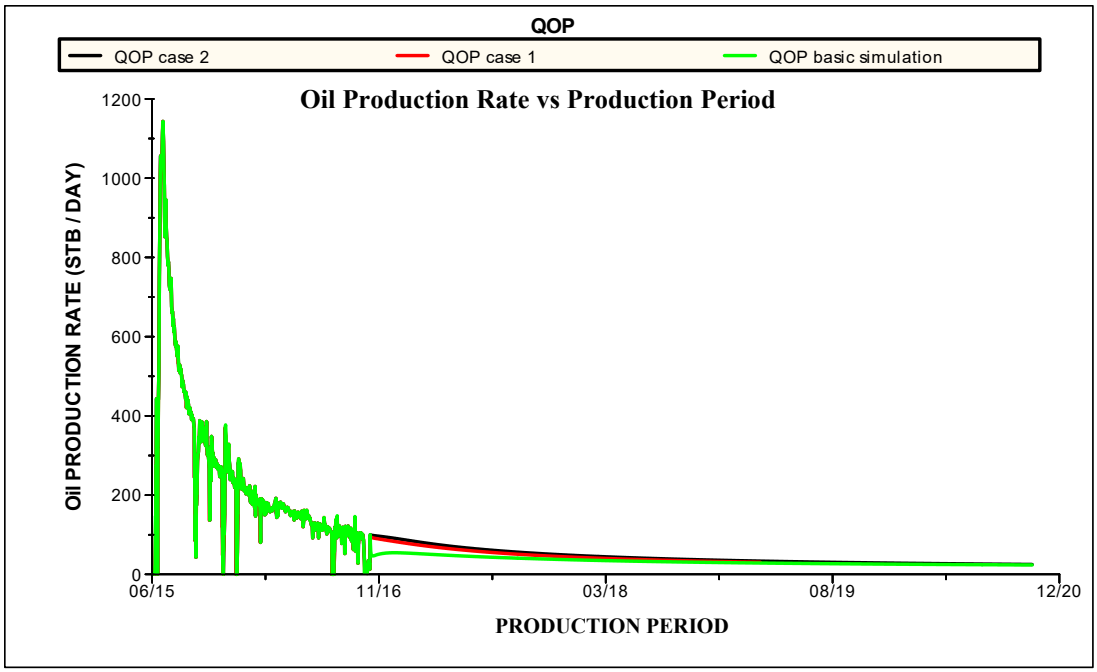


**Figure 4.8: Oil production rates for 5 year simulation run for multiplier approach and EDFM cases**

Cumulative oil production is also underpredicted in the case of multiplier approach as seen in Fig 4.9 whereas gas production is overpredicted as seen in Fig 4.10.

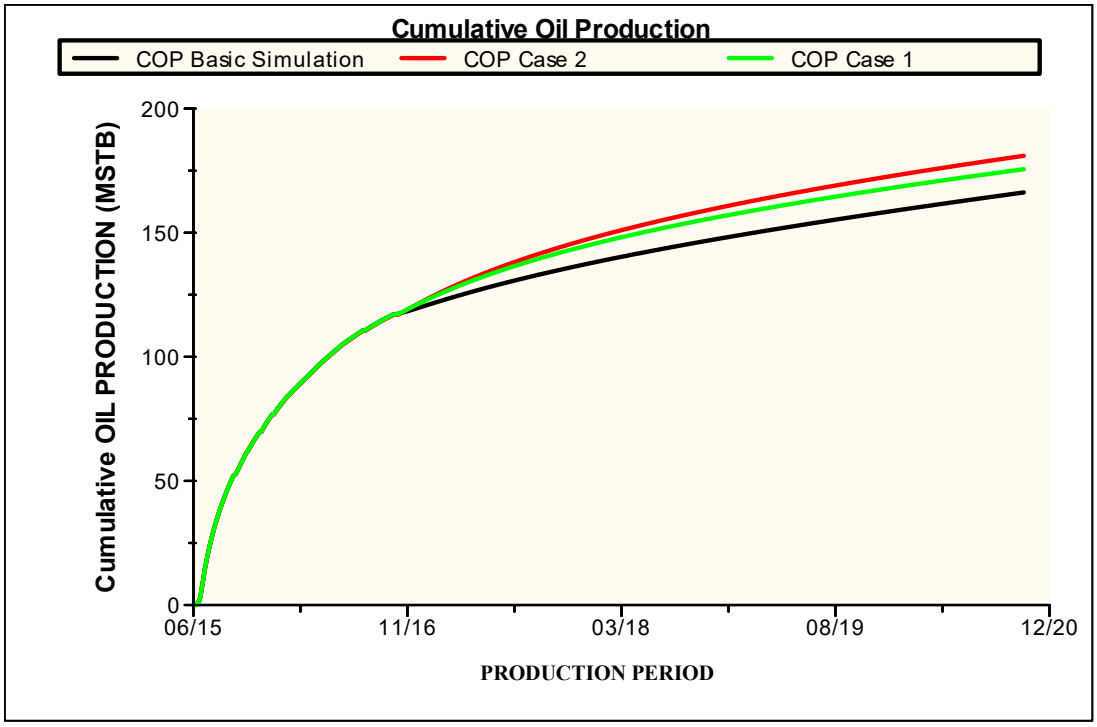


**Figure 4.9: Cumulative Oil Production for 5 year simulation runs**

In Fig 4.11, the average pore pressure for multiplier approach is significantly lower than the EDFM cases. This could be attributed to the use of pore volume multiplier. Hence, it can be argued that the EDFM 5 year responses could be more accurate as they do not involve varying pore volumes for simulation purposes explicitly.

The BHP is best recorded using a bottom hole pressure gauge. Many field cases, including the parent well for which history matching is performed, are devoid of bottom

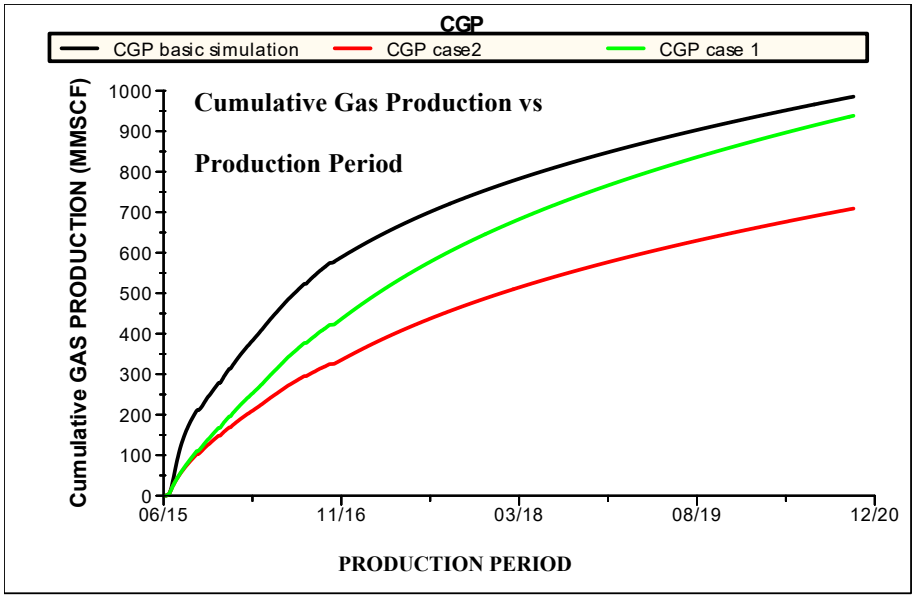


**Figure 4.10: Cumulative Gas Production for 5-year simulation runs**

hole pressure gauges. Hence for production history, the BHP is estimated using the oil flow rates, gas flow rates and well head pressure observed at well head conditions.

Gas migration and expansion along the well contribute to the spike of the bottomhole pressure observed during shut in or near shut-in cases. As the location of the gas bubbles inside the well during shut in is hard to model, the BHP estimated during shut in pressure typically underpredicts the BHP response, as it is estimated based on the gas rates observed at well head.

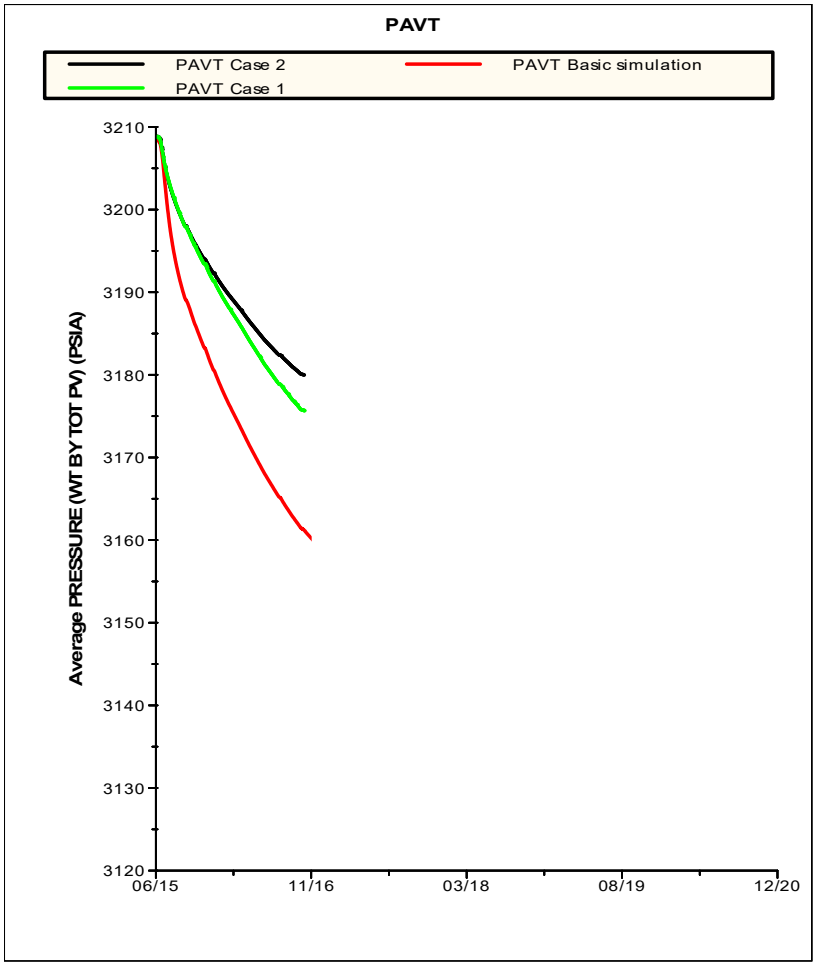


**Figure 4.11: Average pore pressure vs production period for multiplier approach and EDFM approach**

# 5. COMPARING RESULTS WITH LITERATURE

## 5.1. Modeling Interwell Interference Due to Complex Fracture Hits in Eagle Ford Using EDFM (Fiallos, M. X. et al., 2019)

### 5.1.1. Paper Background

In the paper, Modeling Interwell Interference Due to Complex Fracture Hits in Eagle Ford Using EDFM, the results of a numerical black oil model in combination with embedded discrete fracture model are presented and corroborated with proper history matching of a field case from Eagle Ford shale. The subject paper uses a field case with multiple parent and child wells. The model was history matched with flowing bottomhole pressure (BHP) and gas flow rate, using measured oil flow rate as the simulation well constraint. The main objective of the subject paper is to model and study interwell interference and fracture hits which is however outside the scope of this research work.

### 5.1.2. Similarities between the paper and research work

There are plenty of similarities between the work mentioned in the paper and research work performed here

1. Both the reservoirs being modelled (the paper and this research) are black oil shale reservoirs
2. While the paper works on a field case with multiple parent horizontal wells and horizontal infill wells and performs history matching for all the wells, this

research works on a field case which has a single parent horizontal well and more infill wells. History matching is however performed only for the parent well in this research.

3. Both the paper and the research involve simulation of the reservoir by modelling fractures using EDFM.
4. The porosity and permeability values of the field case in the paper and this research are similar. Fig 5.1 shows the range of permeability and porosity values across different layers of the field case used in the paper. We notice that the paper's field case has a range of values for permeability between 0.2 – 0.75μd , which is similar in range the field case used in this research which is 0.3 – 0.9 μd (shown in Table 3.1). Porosity values in the case of the paper range from 4% - 10%, which is similar to the range of porosity values for this research which vary between 2 – 7% as shown in Table 3.1.

| LAYER | 1 | 2 | 3 | 4 | 5 | 6 | 7 |
|---|---|---|---|---|---|---|---|
| Thickness, ft | 12 | 27 | 19 | 20 | 21 | 18 | 13 |
| Permeability, md | 0.0002 | 0.0003 | 0.00045 | 0.0003 | 0.00075 | 0.00065 | 0.00035 |
| Porosity, ratio | 0.045 | 0.07 | 0.08 | 0.1 | 0.1 | 0.085 | 0.04 |

**Figure 5.1:Permeability and porosity values for the field case used in the paper (Fiallos, M. X. et al., 2019)**

### 5.1.3. Differences between the paper and research

1. The work in the paper is centered around modelling interwell interference and fracture hits using EDFM history matching workflow, whereas the objective of

this research work is to model the fracture network and SRV properties of the parent well

2. Even though the paper uses an EDFM workflow, the fractures are modelled as individual planes along the wellbore with variations in strike angle as seen in Fig 5.2. This research however attempts to generate a complex fracture network.
3. The paper does not discuss about fracture conductivity decline during the depletion period

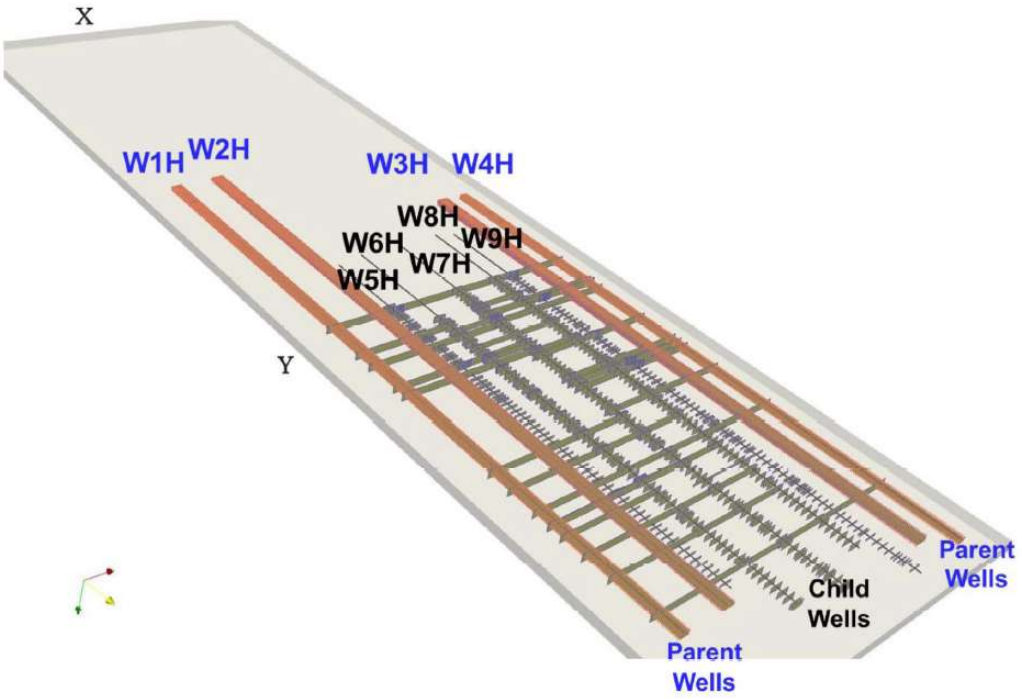


**Figure 5.2: Parent and child well layout of Eagle Ford case. Fracture planes are modelled as planes (Fiallos, M. X. et al., 2019)**

### 5.1.4. Comparing results

Fig 5.3 shows one of the outputs from one of the parent wells. The first six months of the production period here, the average BHP simulated is about 1200psia lower than observed which translates to a 33% average error rate. It also does not accurately periods of shut-in or very low flow rates when BHP is massive shown in circle in Fig 5.3.

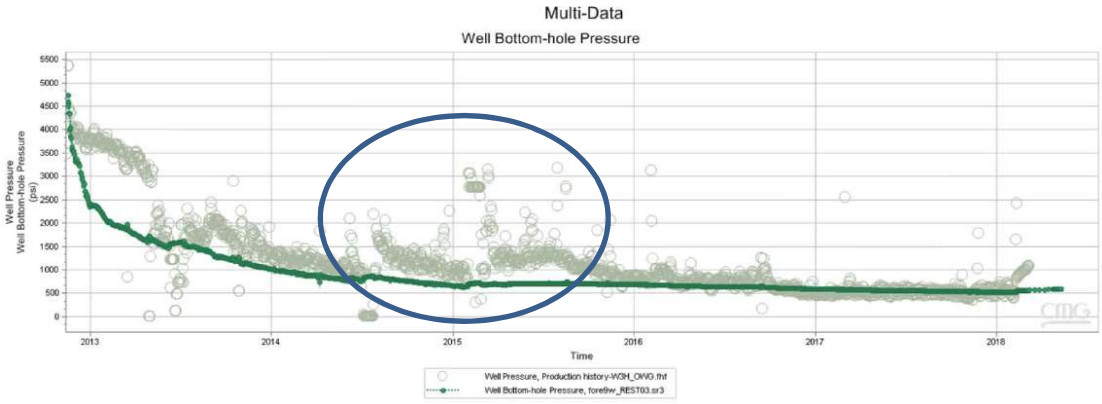


**Figure 5.3: BHP production history and EDFM simulation of Eagle Ford case (Fiallos, M. X. et al., 2019)**

Fig 4.4 shows one of the best EDFM matches used in this research. For the first six months, the average error rate is 6%, indicating a better EDFM match is achieved as compared to the paper for the initial sharp decline period. Fig 5.3 also shows a smooth BHP simulation response as compared to a noisy BHP production history. This weak response could be attributed to modelling the fractures as simple planes along the wellbore. It is observed that the response characteristics are similar to the multiplier approach discussed in section 4.5. This example shows the advantages of building a discrete fracture network model for simulation purposes as built in this research workflow.

The parameters obtained from EDFM history matching in the paper are listed in Fig 5.4 with the parent wells W1H, W2H, W3H and W4H having fracture conductivities in the range of 8-14 md-ft. Even though this research work used a dynamic fracture conductivity, the initial conductivites of 8-12 md-ft are very similar to the results obtained in the paper. The fracture half lengths and fracture heights are of similar magnitude to what is obtained in the case of this research.

| Well | Number of Hydraulic Fractures | Fracture conductivity, md-ft | Fracture half-length, ft | Fracture height, ft |
|---|---|---|---|---|
| W1H | 429 | 6 | 75 | 65 |
| W2H | 429 | 14 | 100 | 45 |
| W5H | 98 | 252 | 75 | 30 |
| W6H | 119 | 8.25 | 75 | 75 |
| W7H | 130 | 4.5 | 65 | 75 |
| W8H | 95 | 360 | 100 | 75 |
| W9H | 121 | 270 | 75 | 30 |
| W3H | 368 | 8 | 70 | 75 |
| W4H | 379 | 10 | 55 | 65 |

**Figure 5.4: EDFM model parameters after successful history match for Eagle Ford case (Fiallos, M. X. et al., 2019)**

## 5.2. Sampling a Stimulated Rock Volume: An Eagle Ford Example (Raterman, K. T., 2017)

### 5.2.1. Background

The paper by ConocoPhillips was to study hydraulic fracturing properties. The work in the paper was based on a pilot design which relied heavily on spatial sampling adjacent to an Eagle Ford horizontal producer, both before and after hydraulic stimulation, to characterize the state of hydraulic fracturing. Remote monitoring by microseismicity and Distributed Acoustic and Temperature Sensing were an integral part of the design. Also included as part of the study was an extensive set of core logs and image logs. Furthermore, the design employed multiple pressure gauges to monitor the spatial progress of depletion with the intent to tie production performance to observed fracture characteristics.

### 5.2.2. Some major observations from the paper and comparing the results obtained

As per the observations noted in the paper, permeability enhancement is realized through discrete fractures rather than distributed matrix damage. The effective reservoir permeability is presumed to be anisotropic. The fractures are not evenly distributed spatially; thus, reservoir drainage may be non-uniform. This observation is broadly respected by the fracture network generated as shown in Fig 4.3 and the drainage is non-uniform. This is directly opposite to multiplier approach which has uniform drainage throughout the wellbore.

The paper also noted that the hydraulic fractures are numerous and broadly parallel. There are many more fractures than perforation clusters. In the areas where the study was conducted, the hydraulic fracture density was observed to decrease above and laterally away from the producer. This indicates that the hydraulically fractured volume could be in the order of two to three times as broad, laterally, as it is tall. This observation is also broadly respected by the EDFM history match models where the fracture height is 75 – 120 feet and fracture lengths of 200-250 feet.

The paper also noted that although the stimulation very efficiently fractured the formation, sometimes up to half lengths of 750 feet, proppant placement was less successful. This is also seen in the case of the research workflow followed here. The initial ensembles were much larger similar to the overlay microseismic cloud. However, as this workflow was modelling only propped fractures and unpropped fractures were ignored, the subsequent ensembles were significantly smaller in volume as compared to the original ensemble. This gives a strong indication that the propped fractures are a small portion as compared to the unpropped fractures.

# 6. CONCLUSIONS AND DISCUSSIONS

This research was successful in achieving good EDFM history match for the field case given. Even though the global average error percentage is around 28%, there is a strong argument to be made that the BHP history, which is actually estimated, is not accurate in modelling the high spikes in BHP during shut in or near shut in due to gas migration. The research workflow was able to successfully model a complex fracture network and achieve better results as compared to models that incorporate fractures as simple planes. Major results were compared to existing literature and most observations with regards to EDFM properties and fracture network properties were broadly supported.

The results also indicate that the microseismic cloud does not provide any valuable information with regards to fracture density or the extent of proppant placement as the final SRV was significantly smaller in volume than the microseismic cloud observed for the child well. The workflow also was able to successfully model fracture conductivity decline, also supporting the understanding that fractures have a rapid closure in the initial days of production after which they no longer provide good conduits for hydrocarbon flow.

Over 500 simulation models over different ensembles were generated, executed and results studied. Such a large model base makes manual history matching harder and there is a definite need to use assisted mathematical history matching workflows in the future for similar studies.

The computing efficiency of EDFM is best exhibited here as the field case of 480 days takes only about 2.5 mins on a 12 gigabyte memory laptop. This combined with the numerical accuracy makes EDFM a powerful tool to study hydraulic fracturing in horizontal wells. This research also provides the framework to study infill wells, fracture hits and well interference.

# REFERENCES


Aarseth, E. S., Bourgine, B., Castaing, C., Chiles, J. P., Christensen, N. P., Eeles, M., ... & Jørgensen, K. Z. (1997). Interim guide to fracture interpretation and flow modelling in fractured reservoirs. European Commision Eur 17116 En, 1-203.

Chai, Z., Yan, B., Killough, J. E., & Wang, Y. (2016, November 12). Dynamic Embedded Discrete Fracture Multi-Continuum Model for the Simulation of Fractured Shale Reservoirs. International Petroleum Technology Conference. doi:10.2523/IPTC-18887-MS

Cipolla, C.L., Warpinski, N.R., Mayerhofer, et al., 2008. The relationship between fracture complexity, reservoir properties, and fracture treatment design. SPE Prod. Oper. 25 (04) SPE-115769. https://doi.org/10.2118/115769-PA.

Fiallos, M. X., Yu, W., Ganjdanesh, R., Kerr, E., Sepehrnoori, K., Miao, J., & Ambrose, R. (2019, March 22). Modeling Interwell Interference Due to Complex Fracture Hits in Eagle Ford Using EDFM. International Petroleum Technology Conference. doi:10.2523/IPTC-19468-MS

Gale, J. F., Laubach, S. E., Olson, J. E., Eichhubl, P., & Fall, A. (2014). Natural fractures in shale: A review and new observationsNatural Fractures in Shale: A Review and New Observations. AAPG bulletin, 98(11), 2165-2216.

Gillespie, P. A., Howard, C. B., Walsh, J. J., & Watterson, J. (1993). Measurement and characterisation of spatial distributions of fractures. Tectonophysics, 226(1-4), 113-141. doi: 10.1016/0040-1951(93)90114-Y

Hajibeygi, H., Karvounis, D., and Jenny, P., 2011, A hierarchical fracture model for the iterative multiscale finite volume method, Journal of Computational Physics, Vol.230, 8729-8743.

Heinemann, Z. E., Brand, C., Munka, M., & Chen, Y. M. (1989, January 1). Modeling Reservoir Geometry With Irregular Grids. SPE. doi:10.2118/18412-MS

Kanamori, H., 1977. The energy release in great earthquakes. J. Geophys. Res. 82 (20), 2981–2987 ISSN 0148–0227.

Karimi-fard, M., Durlofsky, L.J., and Aziz, K., 2004, An efficient discrete-fracture model applicable for general purpose reservoir simulators, SPE Journal, Vol. 9, 227-236.

Lee, S. H., Jensen, C. L., & Lough, M. F. (2000, September 1). Efficient Finite-Difference Model for Flow in a Reservoir With Multiple Length-Scale Fractures. SPE. doi:10.2118/65095-PA

Li, L., & Lee, S. H. (2008, August 1). Efficient Field-Scale Simulation of Black Oil in a Naturally Fractured Reservoir Through Discrete Fracture Networks and Homogenized Media. SPE. doi:10.2118/103901-PA

Moinfar, A., Varavei, A., Sepehrnoori, K., & Johns, R. T. (2014, April 1). Development of an Efficient Embedded Discrete Fracture Model for 3D Compositional Reservoir Simulation in Fractured Reservoirs. SPE. doi:10.2118/154246-PA

Mustapha, H. (2014). A Gabriel-Delaunay triangulation of 2D complex fractured media for multiphase flow simulations. Computational Geosciences, 18(6), 989-1008. https://doi.org/10.1007/s10596-014-9440-0

Odling, N. E., Gillespie, P., Bourgine, B., Castaing, C., Chiles, J. P., Christensen, N. P., ... & Trice,R. (1999). Variations in fracture system geometry and their implications for fluid flow in fractures hydrocarbon reservoirs. Petroleum Geoscience, 5(4), 373-384.

Ouillon, G., Castaing, C., & Sornette, D. (1996). Hierarchical geometry of faulting. Journal of Geophysical Research: Solid Earth, 101(B3), 5477-5487. doi: 10.1029/95JB02242

Orta, Samuel Rene (2017). 3D Reservoir Simulation of a Hydraulically Fractured Vertical Gas Well Using the Embedded Discrete Fracture Model (EDFM). Master's thesis, Texas A & M University. Available electronically from http:/ /hdl.handle.net/1969.1/166075.

Peaceman, D.W., 1983, Interpretation of well-block pressures in numerical reservoir simulation with non-square grid blocks and anisotropic permeability, SPE Journal, Vol. 23, 531-543.

Raterman, K. T., Farrell, H. E., Mora, O. S., Janssen, A. L., Gomez, G. A., Busetti, S., … Warren, M. (2017, July 24). Sampling a Stimulated Rock Volume: An Eagle Ford Example. Unconventional Resources Technology Conference. doi:10.15530/URTEC-2017-2670034

Sandve, T. H., Berre, I., & Nordbotten, J. M. (2012, May 1). An Efficient Multi-Point Flux Approximation Method for Discrete Fracture-Matrix Simulations. Journal of Computational Physics, 231, 3784–3800. doi:10.1016/j.jcp.2012.01.023

Sun, J., Schechter, D., & Huang, C.-K. (2015, November 9). Sensitivity Analysis of Unstructured Meshing Parameters on Production Forecast of Hydraulically Fractured Horizontal Wells. SPE. doi:10.2118/177480-MS

Seibel, M., Baig, A., & Urbancic, T. (2010, January 1). Single Versus Multiwell Microseismic Recording: What Effect Monitoring Configuration Has On Interpretation. Society of Exploration Geophysicists.

Siriwardane, H.; Gondle, R.; Bromhal, G. Extent of Hydraulic Fractures in Shales; NETL-TRS-16-2016; NETL Technical Report Series; U.S. Department of Energy, National Energy Technology Laboratory: Morgantown, WV, 2016; p 52.

Williams-Stroud, S.C., 2008. Using microseismic events to constrain fracture network models and implications for generating fracture flow properties for reservoir simulation. In: SPE Shale Gas Production Conference, Fort Worth, Texas, USA, 16–18 November, SPE-119895-MS, .https://doi.org/10.2118/119895-MS.

Wu, K. and Olson, J. E. 2014. Mechanics Analysis of Interaction Between Hydraulic and Natural Fractures in Shale Reservoirs. Presented at the SPE/AAPG/SEG Unconventional Resources Technology Conference, Denver, Colorado, 25-27 August. SPE-2014-1922946-MS. http://dx.doi.org/10.15530/urtec-2014-1922946.

Wu, W., Kakkar, P., Zhou, J., Russell, R., & Sharma, M. M. (2017, January 24). An Experimental Investigation of the Conductivity of Unpropped Fractures in Shales. SPE. doi:10.2118/184858-MS

Yu, W., Luo, Z., Javadpour, F., et al., 2014. Sensitivity analysis of hydraulic fracture geometry in shale gas reservoirs. J. Petrol. Sci. Eng. 113, 1–7.

Zheng, S., Kumar, A., Gala, D. P., Shrivastava, K., & Sharma, M. M. (2019, July 25). Simulating Production from Complex Fracture Networks: Impact of Geomechanics and Closure of Propped/Unpropped Fractures. Unconventional Resources Technology Conference. doi:10.15530/urtec-2019-21